

Frequency filtering in disordered granular chains

Brian P. Lawney, Stefan Luding
Multiscale Mechanics (MSM), MESA+,
Faculty of Engineering Technology (CTW),
PO Box 217, 7500 AE Enschede, Netherlands

July 11, 2013

Abstract

The study of disorder induced frequency filtering is presented for one-dimensional systems composed of random, pre-stressed masses interacting through both linear and nonlinear (Hertzian) repulsive forces. An ensemble of such systems is driven at a specified frequency and the spectral content of the propagated disturbance is examined as a function of distance from the source. It is shown that the transmitted signal contains only low-frequency components and the attenuation is dependent on the magnitude of disorder, the input frequency, and the contact model. It is found that increased disorder leads to a narrower bandwidth of transmitted frequencies at a given distance from the source and that lower input frequencies exhibit less sensitivity to the arrangement of the masses. Comparison of the nonlinear and linear contact models reveals qualitatively similar filtering behavior; however, it is observed that the nonlinear chain produces transmission spectrums with a greater density at the lowest frequencies. In addition, it is shown that random masses sampled from normal, uniform, and binary distributions produce quantitatively indistinguishable filtering behavior, suggesting that only knowledge of the distribution's first two moments is sufficient to characterize the bulk signal transmission behavior. Finally, we examine the wavenumber evolution of random chains constrained to move between fixed end-particles and present a transfer matrix theory in wave-number space, and an argument for the observed filtering based on the spatial localization of the higher-frequency normal modes.

1 Introduction

One-dimensional analogs of electronic, magnetic, and mechanical systems are often employed for their use as simple models which have the potential to reveal the physics of more general, higher dimensional systems [20]. As a subset of these problems, chains of non-cohesive particles have received significant attention in the literature. Linear arrangements of harmonic oscillators are common in the introduction to lattice vibrations in solid state physics [11,41]. These treatments are typically limited to infinitely repeatable unit cells containing one or two particles/atoms for which dispersion equations relating the oscillation frequency and wavelength are analytically accessible. It is from these periodic, linear

systems that more recent studies on inhomogeneous, disordered, and nonlinear chains originate.

The introduction of nonlinear (e.g., Hertzian) particle interactions resembles most experiments with granular chains of pre-stressed elastic spheres, and leads to novel behavior such as soliton-like nonlinear waves [2, 16, 22–24, 29, 35]. Sen *et al.* [34] provides a detailed account of prior studies concerning solitary waves in granular chains. Note that many studies focus on uncompressed chains where particles are barely in contact. Additionally, there is significant attention placed on the behavior of “designed” and ordered nonlinear chains, often motivated by energy modification and shock-protection applications. Studies have employed smoothly varying mass distributions [31], “decoration” (e.g. deliberate insertion of different sized masses) [9, 12, 13], tapering [5, 25, 38, 40], and controlled variation of the particle material [3, 14]. Combinations of both tapering and decoration have also been employed [6, 12].

The inclusion of disorder through mass, size, or interaction (stiffness) variation (and combinations thereof) is a natural extension reflecting the disordered, inhomogeneous state of many realistic discrete systems. One-dimensional systems provide a simple framework to study the basic effects of disorder without consideration for the geometric complexity of higher dimensions, thus excluding the scattering of signals to other directions. Analysis of the spectrum and density of eigenstates was the subject of many early studies in disordered one-dimensional systems [4, 7, 26, 33]. In the context of quantum mechanical particles, Anderson [1] noted the localization of the wavefunctions in the presence of sufficiently strong random potentials. This “Anderson localization” has been confirmed in disordered mechanical systems of vibrating masses [19, 32].

As with tapered and decorated chain arrangements, recent studies of random granular arrays show an interest in the use of these systems to dissipate or enhance energy propagation. Nesterenko [29] examined the downstream speed and energy of particles in nonlinear random chains following an initial excitation applied to one end of the system. It was reasoned that complex nonlinear interactions between the chain members make the system behavior difficult to predict in general. Manciu *et al.* [24] reports a spatially exponential decrease of the incident kinetic energy for various amounts of mass disorder, with increasing disorder leading to a faster energy loss. Fraternali *et al.* [8] employed an evolutionary algorithm which generated random “protecting” chains whose effectiveness was evaluated by the force transmitted at the end of the system. It was noted that temporally short and high amplitude pulses were transformed to low amplitude, longer wavelength (temporally longer) signals at the downstream receiver. Ponson *et al.* [30] employs a nonlinear chain of two-particle unit cells which are randomly oriented, as in a spin system, and studies the effect of their disorder parameter on the spatial decay of the force transmitted by such systems. Harbola *et al.* [13] decorate monodisperse chains with randomly sized small masses and investigate the propagation time and decay of the pulse velocity as a function of system penetration.

Studies concerning the frequency-filtering effects of disorder have received less attention than energy or force attenuation. Jia *et al.* [15] reports experimental studies on ultrasound propagation through three-dimensional packings of glass beads. The time and frequency analysis of the transmitted signal reveals the appearance of an initial pulse close to the source that contains relatively low frequencies with respect to the input spectrum. The initial pulse is followed

by an irregular signal, *i.e.* the “coda”, that contains the higher frequencies, consistent with the lower phase velocity of higher frequency components. The spectrum of this irregular signal seems to indicate more attenuation of the high frequency components. Judge *et al.* [17] numerically examine the spectra of disordered micromechanical oscillators, focusing on frequency filtering within the passband of ordered arrays. They note the significant change in the transmitted spectrum with increasing disorder and the propagation of frequencies associated with the natural frequency of the individual oscillators. The low-pass filtering seen does not seem to be observed, likely due to the short length of the arrays considered (5 oscillators). Mouraille and Luding [27,28] numerically studied the high-frequency filtering present in three-dimensional packings perturbed from their perfect crystalline geometry by a small random variation in the particle sizes. Following a delta-like pulse of the boundary, only the low-frequency components of the excitation are observed to propagate a significant distance. The polydispersity introduced is quite small with respect to the particle length scale (0.2% variation), but as this change is comparable to the contact length scale remarkable differences in the propagation characteristics of the medium are observed.

It is worth noting that nonlinear particle interactions permit frequency mixing behavior. Given excitations at frequencies ω_1 and ω_2 , a component at the difference-frequency $|\omega_2 - \omega_1|$ is generated, among others. For sufficiently close magnitudes, this is a low-frequency component. In realistic materials, the high-frequencies are attenuated and only the difference-frequency is seen to propagate a significant distance. Tournat *et al.* [39] observe the propagation of these low-frequency signals in nonlinear chains, terming it self de-modulation. However, such behavior is due to nonlinear interaction and is not a mass-disorder induced effect. Frequency mixing due to disorder was also noted by Mouraille [27].

In this paper we study the effect of disorder and non-linearity on the transmission of signals in one-dimensional systems. We consider initially static, pre-stressed configurations with given disorder magnitude that are subjected to a harmonic perturbation of the boundary. Prescribing a perturbation frequency, we average over many configurations of the chain to observe ensemble averaged behavior. In section 2 we derive the equations of motion that govern the idealized system. In particular, the linear and Hertzian force models are given in sections 2.1.2 and 2.1.3, respectively. Using these relations, we examine the effects of disorder on the high-frequency filtering behavior in section 3, and summarize and conclude in Section 4.

2 Modeling

In this section the equations of motion are derived employing a general nonlinear force-displacement relation. Two specific cases follow, corresponding to the harmonic (linear) and Hertzian models.

2.1 Compressed chain

In this study we consider one-dimensional arrays of $(N + 2)$ random mass particles which interact with only their immediate neighbors in a purely repulsive manner. In addition, we consider chains that are pre-compressed such that

there is some initial strain associated with the equilibrium configuration. The absolute position, radius, and mass of a general particle j are given by $\tilde{x}^{(j)}$, $\tilde{r}^{(j)}$, and $\tilde{m}^{(j)}$, respectively. Anticipating an appropriate scaling of the problem, we employ the tilde symbols to denote dimensional quantities. The interaction force between neighboring particles i and j is modeled as,

$$\left| \tilde{F}_{(i,j)} \right| = \tilde{\kappa}_{(i,j)} \tilde{\delta}_{(i,j)}^{1+\beta}, \quad \tilde{\delta}_{(i,j)} \geq 0, \quad (1)$$

where $\tilde{\kappa}_{(i,j)}$ is a “stiffness” that changes with the value of β and depends, in general, on the properties of the contacting bodies. The particle overlap is given as $\tilde{\delta}_{(i,j)} = \tilde{r}^{(i)} + \tilde{r}^{(j)} - |\tilde{x}^{(j)} - \tilde{x}^{(i)}|$ such that it is strictly non-negative for contacts. The Hertz and linear models are given by $\beta = 1/2$ and $\beta = 0$, respectively [18, 21, 29]. Choosing a length scale $\tilde{\ell}$ (to be determined later) we scale the particle overlap:

$$\left| \tilde{F}_{(i,j)} \right| = \tilde{\kappa}_{(i,j)} \tilde{\ell}^{1+\beta} \delta_{(i,j)}^{1+\beta}, \quad (2)$$

where $\delta_{(i,j)} \equiv \tilde{\delta}_{(i,j)}/\tilde{\ell}$. Compressing the chain by an applied force \tilde{P} , the dimensionless initial particle overlap at the contact between i and j is,

$$\Delta_{(i,j)} = \left(\frac{\tilde{P}}{\tilde{\kappa}_{(i,j)} \tilde{\ell}^{1+\beta}} \right)^{1/(1+\beta)}. \quad (3)$$

Associated with the length scale $\tilde{\ell}$, we have a characteristic mass \tilde{m}_o , which we take as the mean particle mass of the system. Dimensional analysis yields a time scale,

$$\tilde{t}_c = \frac{1}{\tilde{\ell}^{\beta/2}} \sqrt{\frac{\tilde{m}_o}{\tilde{\kappa}_o}}, \quad (4)$$

where $\tilde{\kappa}_o$ functions as the characteristic stiffness of the system. This will be defined with respect to the contact of two identical particles of the mean mass, \tilde{m}_o . In the nonlinear cases ($\beta \neq 0$) $\tilde{\ell}$ factors into this time scale. We may write an equation of motion for the general particle i ($i = 1, \dots, N$) as:

$$\tilde{m}^{(i)} \frac{d^2 \tilde{x}^{(i)}}{d\tilde{t}^2} = \tilde{\kappa}_{(i-1,i)} \tilde{\ell}^{1+\beta} \delta_{(i-1,i)}^{1+\beta} - \tilde{\kappa}_{(i+1,i)} \tilde{\ell}^{1+\beta} \delta_{(i+1,i)}^{1+\beta}. \quad (5)$$

We denote the displacement of particle i from its equilibrium position $\tilde{x}_o^{(i)}$ as $\tilde{u}^{(i)} = \tilde{\ell} u^{(i)} = \tilde{x}^{(i)} - \tilde{x}_o^{(i)}$. Thus, for a contact between i and j (with $j > i$) the scaled overlap is $\delta_{(i,j)} = \Delta_{(i,j)} - (u^{(j)} - u^{(i)})$. With dimensionless mass $b^{(i)} \equiv \tilde{m}^{(i)}/\tilde{m}_o$ and time $\tau \equiv \tilde{t}/\tilde{t}_c$ we write

$$b^{(i)} \frac{d^2 u^{(i)}}{d\tau^2} = \kappa_{(i-1,i)} \left[\Delta_{(i-1,i)} - u^{(i)} + u^{(i-1)} \right]^{1+\beta} - \kappa_{(i+1,i)} \left[\Delta_{(i+1,i)} + u^{(i)} - u^{(i+1)} \right]^{1+\beta}, \quad (6)$$

where the stiffness ratio $\kappa_{(i,j)} = \tilde{\kappa}_{(i,j)}/\tilde{\kappa}_o$ has been defined implicitly.

For the particles 1 and N we write equations of motion associated with the imposed boundary conditions. We harmonically displace particle 0 at angular frequency $\omega_o = \tilde{\omega}_o \tilde{t}_c$ and fix particle $(N+1)$:

$$u^{(0)}(\tau) = \epsilon \sin \omega_o \tau, \quad (7)$$

$$u^{(N+1)}(\tau) = 0, \quad (8)$$

where $\epsilon = \tilde{\epsilon}/\tilde{\ell}$ is the scaled oscillation amplitude. Thus, the coupled system of differential equations governing the modeled system is given by (6) with substitution of (7) and (8) for $i = 1$ and $i = N$, respectively.

There are various choices available for the length scale $\tilde{\ell}$. One could use the particle size or the driving amplitude. However, we choose the length scale to be related to the overlap of a characteristic contact in static equilibrium. As in defining the characteristic stiffness, we consider the contact of two identical particles of the mean mass. Under the applied compressive force, the initial overlap between such particles provides us with $\tilde{\ell} = \tilde{\Delta}_o$ ($\Delta_o = 1$). In a typical simulation, the scaled driver amplitude $\epsilon \ll \Delta_o$ is chosen so as not to cause an opening of contacts. However, we explore driver amplitudes that approach the contact length scale under the restriction that particles remain in contact at all times. Note that ϵ incorporates the pre-compression of the system through (3):

$$\epsilon = \frac{\tilde{\epsilon}}{\tilde{\Delta}_o} = \tilde{\epsilon} \left(\frac{\tilde{\kappa}_o}{\tilde{P}} \right)^{2/3}. \quad (9)$$

Since $\tilde{\kappa}_o$ is set by the size of the particles (see Appendix B), small values of ϵ represent systems with small driving and/or a large pre-stress through \tilde{P} .

2.1.1 Linearized equations of motion:

Here we linearize the general force-displacement relation about the equilibrium configuration. The non-dimensional phrasing of (1) is given by

$$F_{(i,j)}(\delta_{(i,j)}) = \kappa_{(i,j)} \delta_{(i,j)}^{1+\beta}, \quad (10)$$

Expanding about the equilibrium position $\Delta_{(i,j)}$ we obtain,

$$F_{(i,j)}(\delta_{(i,j)}) = \kappa_{(i,j)} \Delta_{(i,j)}^{1+\beta} + \kappa_{(i,j)} (1 + \beta) \Delta_{(i,j)}^{\beta} (\delta_{(i,j)} - \Delta_{(i,j)}) + \frac{\kappa_{(i,j)} \beta (1 + \beta) \Delta_{(i,j)}^{\beta-1}}{2} (\delta_{(i,j)} - \Delta_{(i,j)})^2 + \dots \quad (11)$$

Assuming small displacements from equilibrium, we retain only the constant and linear terms. With $\delta_{(i,j)} = \Delta_{(i,j)} - (u^{(j)} - u^{(i)})$ for particle indices such that $j > i$ we obtain

$$F_{(i,j)}(\delta_{(i,j)}) = \kappa_{(i,j)} \Delta_{(i,j)}^{1+\beta} - \kappa_{(i,j)} (1 + \beta) \Delta_{(i,j)}^{\beta} (u^{(j)} - u^{(i)}), \quad (12)$$

which is the linearized force of particle i on particle j for $j > i$. The equation of motion for a general particle i is then,

$$b^{(i)} \frac{d^2 u^{(i)}}{d\tau^2} = \kappa_{(i-1,i)} \Delta_{(i-1,i)}^{\beta} \left[\Delta_{(i-1,i)} - (1 + \beta)(u^{(i)} - u^{(i-1)}) \right] - \kappa_{(i+1,i)} \Delta_{(i+1,i)}^{\beta} \left[\Delta_{(i+1,i)} - (1 + \beta)(u^{(i+1)} - u^{(i)}) \right]. \quad (13)$$

2.1.2 Linear coupling: $\beta = 0$

In the case of $\beta = 0$ we recover the harmonic chain with linear springs between the mass elements. The linear contact model is appropriate for chains with sufficiently high confining force; Sinkovits *et al.* [37] show that the frequency spectrum of oscillations approaches that of a harmonic chain with increasing compressive force. As expected, the general equations of motion (6) and the linear expansion (13) match exactly. We may compactly express the N linear equations in the matrix form

$$\mathbf{M} \frac{d^2 \mathbf{u}}{d\tau^2} = \mathbf{K} \mathbf{u} + \mathbf{f}, \quad (14)$$

where \mathbf{M} is a diagonal matrix with the random mass ratios $b^{(1)}$ through $b^{(N)}$ on the diagonal, and \mathbf{K} is a symmetric, tri-diagonal matrix. The sub- and superdiagonal elements are given by $\mathbf{K}(i, i-1) = \kappa_{(i-1,i)}$ and $\mathbf{K}(i, i+1) = \kappa_{(i+1,i)}$, respectively. The diagonal entries are $\mathbf{K}(i, i) = -(\kappa_{(i-1,i)} + \kappa_{(i+1,i)})$. Since the stiffnesses depend on the contacting particles, these values are random in general. The forcing vector \mathbf{f} has only one non-zero entry, which is $f_1(\tau) = \epsilon \sin \omega_o \tau$ in the first position. Other entries cancel by the equilibrium condition $\kappa_{(i-1,i)} \Delta_{(i-1,i)} = \kappa_{(i+1,i)} \Delta_{(i+1,i)}$.

Since we look to examine the effect of mass disorder alone, we take all coupling stiffnesses to be independent of the contact ($\kappa_{(i,j)} = 1$). Accordingly, all initial overlaps are equal with $\Delta_{(i,j)} = 1$. With this assumption, the stiffness matrix simplifies, with \mathbf{K} now having entries of -2 on the diagonal and entries of $+1$ on the sub and superdiagonal.

We examine the solutions of the linear system (14) in section 2.2.

2.1.3 Nonlinear Hertzian coupling: $\beta = 1/2$

With $\beta = 1/2$ we obtain the Hertz contact model and the equations of motion are given by (6), (7), and (8). The interparticle forces are dependent on the size and material properties of the constituent particles (see Appendix B). We find that the scaled stiffness $\kappa_{(i,j)}$ and initial overlap $\Delta_{(i,j)}$ are given by

$$\kappa_{(i,j)} = \sqrt{\frac{2}{b^{(i)1/3} + b^{(j)1/3}}} \left(b^{(i)} b^{(j)} \right)^{1/6}, \quad (15)$$

and

$$\Delta_{(i,j)} = \kappa_{(i,j)}^{-2/3}. \quad (16)$$

As in the linearized version of the Hertz chain of given by (14), the nonlinear chain of polydisperse spheres is, in general, disordered in both mass and coupling stiffness.

2.1.4 Creation of mass-disordered, monodisperse chains

A general polydisperse chain of masses will be disordered in mass and interparticle contact stiffness. If we wish to remove the effects of this ‘‘contact disorder’’ (as present in the Hertzian model) one may consider the modification of particles to create a monodisperse (size) chain of varied mass. In this manner we isolate the effect of mass disorder. Numerically incorporating such a construction is

trivial; the equations of motion are given by (6), (7), and (8) and we assign $\kappa_{(i,j)} = 1$ and $\Delta_{(i,j)} = 1$ for all contacts (i,j) . In an experimental realization, one may imagine creating such a monodisperse, mass-disordered chain by the removal of material from the particle centers or the inclusion of denser cores. Since the Hertz model is based on deformations local to the contacting surfaces, this change of mass should have a negligible effect on the contact stiffnesses provided the modification is sufficiently far from the surface.

2.2 Linear model– analysis

With the goal of solving for the general motion of the linear chain under the imposed boundary conditions, we look to state (14) in its eigenvector basis. This transformation decouples the equations of motion into N independent relations, facilitating the process of finding a general solution. Upon determination of the solution in the eigensystem, a simple linear transformation yields the motion of the particles.

Thus we first seek to determine the eigenvectors and eigenfrequencies associated with (14). We set $\mathbf{f} = \mathbf{0}$ and assume that for each normal mode all masses oscillate with a particular frequency ω . Defining $\mathbf{A} \equiv -\mathbf{M}^{-1}\mathbf{K}$ (not symmetric, in general) we arrive at the familiar eigenvalue problem:

$$\mathbf{A}\mathbf{u} = \omega^2\mathbf{u}. \quad (17)$$

This may be solved numerically to determine the set of N orthonormal eigenmodes $\{\mathbf{s}_{(j)}\}$ and eigenfrequencies $\{\omega_{(j)}\}$. We normalize the eigenvectors to have the following orthonormality conditions (see Appendix A):

$$\mathbf{s}_{(i)}^T \mathbf{M} \mathbf{s}_{(j)} = \delta_{ij}, \quad (18)$$

where δ_{ij} is the usual Kronecker delta symbol.

We sort the eigenvectors by increasing order of their associated eigenvalues (frequencies) and assemble the $(N \times N)$ matrix \mathbf{S} such that the j^{th} column is eigenvector $\mathbf{s}_{(j)}$. Using \mathbf{S}^{-1} as the transformation matrix between the particle displacements \mathbf{u} and the eigenmode amplitudes \mathbf{z} , we have $\mathbf{z} = \mathbf{S}^{-1}\mathbf{u}$. We also note the similarity transform $\mathbf{S}^{-1}\mathbf{A}\mathbf{S} = \mathbf{D}$, where \mathbf{D} is a diagonal matrix with the (increasing) eigenvalues along the diagonal.

With the use of \mathbf{S} we transform the general equation of motion (14) and obtain the decoupled form:

$$\frac{d^2\mathbf{z}}{d\tau^2} = -\mathbf{D}\mathbf{z} + \mathbf{h}, \quad (19)$$

where $\mathbf{h} = \mathbf{S}^{-1}\mathbf{M}^{-1}\mathbf{f}$. In our specific case of harmonic driving, the transformed forcing vector \mathbf{h} may be rephrased as follows. Since $\mathbf{f} = \epsilon \sin \omega_o \tau \mathbf{e}_1$ ($\mathbf{e}_1 = [1 \ 0 \ \dots \ 0]^T$) we have

$$\mathbf{h} = \mathbf{S}^{-1}\mathbf{M}^{-1}\epsilon \sin \omega_o \tau \mathbf{e}_1 = \epsilon \sin \omega_o \tau \mathbf{y}, \quad (20)$$

where $b^{(1)}\mathbf{y} \equiv \mathbf{S}^{-1}\mathbf{e}_1$ is the first column of \mathbf{S}^{-1} . Exploiting the orthogonality given in (18) we left-multiply \mathbf{y} by $\mathbf{S}^T\mathbf{M}\mathbf{S} = \mathbf{I}$ and find $\mathbf{y} = \mathbf{S}^T\mathbf{e}_1$. Thus \mathbf{y} is the first *row* of \mathbf{S} .

The general solution to (19) is then,

$$\mathbf{z} = \mathbf{C}^{(1)}\mathbf{a}^{(1)} + \mathbf{C}^{(2)}\mathbf{a}^{(2)} + \epsilon \sin \omega_o \tau \mathbf{c}, \quad (21)$$

where $\mathbf{C}^{(1)}$ and $\mathbf{C}^{(2)}$ are diagonal matrices with (j, j) entries $\sin \omega_j \tau$ and $\cos \omega_j \tau$, respectively. The vectors $\mathbf{a}^{(1)}$ and $\mathbf{a}^{(2)}$ are determined from the initial conditions of the displacement $\mathbf{u}(0) = \mathbf{u}_o$ and velocity $\dot{\mathbf{u}}(0) = \mathbf{v}_o$. Vector \mathbf{c} has j^{th} entry $S_{1j}/(\omega_j^2 - \omega_o^2)$. Employing the initial conditions we obtain,

$$\mathbf{a}^{(1)} = \mathbf{W}^{-1}\mathbf{S}^{-1}\mathbf{v}_o - \epsilon \omega_o \mathbf{W}^{-1}\mathbf{c}, \quad (22)$$

$$\mathbf{a}^{(2)} = \mathbf{S}^{-1}\mathbf{u}_o. \quad (23)$$

Here, \mathbf{W}^{-1} is a diagonal matrix with $1/\omega_{(j)}$ as the (j, j) entry. If we specify initial conditions $\mathbf{u}_o = \mathbf{v}_o = \mathbf{0}$ and transform back to displacement space via \mathbf{S} , we obtain the displacement history of particle p ,

$$u^{(p)}(\tau) = \epsilon \sum_{j=1}^N \frac{S_{pj}S_{1j}}{(\omega_{(j)}^2 - \omega_o^2)} \left(\sin \omega_o \tau - \frac{\omega_o}{\omega_{(j)}} \sin \omega_{(j)} \tau \right). \quad (24)$$

For a given chain arrangement, we may calculate the displacement history from (24) and this way investigate the frequency spectrum at a particular location in the chain. Discussion of the terms in (24) is deferred to section 3.3.

We finally note that in the case of an undriven ($\epsilon = 0$) monodisperse linear chain, we obtain the dispersion relation [41],

$$\omega(k) = 2 \sin(k^*), \quad (25)$$

where $k^* = d_0 k = 2\pi d_0/\lambda$ is the dimensionless wavenumber (purely real) scaled by the particle diameter. This sets the cutoff frequency for propagative waves at $\omega \leq \omega_{max} = 2$. At $\omega_{max} = 2.0$ we have the minimum scaled wavelength $\lambda_{min}^* = \lambda/d_0 = 2$. That is, signal frequency components in the passband of $0 < \omega \leq 2$ propagate without attenuation. Frequencies above the cutoff are termed evanescent waves as the wavenumber has an imaginary component which causes the signal to exponentially decay with distance. Since our random chains contain masses distributed about the monodisperse system of $b^{(i)} = 1$ we will consider driving frequencies ω_o on the order of $\omega = 2$, in the range $[0.1\omega_{max}, 1.6\omega_{max}]$.

3 Results and Discussion

In this section we present results on the high-frequency filtering effects of random chains.

Section 3.1 discusses the construction of the random systems for several mass distributions. We also introduce our definition of the disorder parameter.

Section 3.2.1 contains results for the chain with linear contact forces, with masses chosen from a normal mass distribution and uniform contact stiffness, examining the effects of disorder and driving frequency. A comparison of mass distributions is shown in 3.2.2, and section 3.2.3 investigates the role of coupling (contact stiffness) disorder in harmonic chains.

Results related to the nonlinear chain are presented in section 3.4. Similar to the linear chain we perform a parameter study in section 3.4.1 and examine

the effect of disorder and driving frequency. The driving amplitude is also considered. We follow this in section 3.4.2 with results for the nonlinear chain featuring uniform contact interactions, which isolates the effect of mass disorder.

3.1 Chain generation

We introduce mass disorder to the chains by randomly sampling from a specified probability distribution. A seeded random number generator with the appropriate statistical properties is created to generate the masses. In this study we consider normal $f^{(n)}(b)$, uniform $f^{(u)}(b)$, and binary discrete $f^{(d)}(b)$ distributions, where b is the scaled mass.

For the normal distribution of masses, we prescribe the mean $\bar{b} = 1$ and standard deviation ξ , which will be used to quantify the disorder of the system. When sampling masses to create the normally distributed random chains, we enforce a lower cutoff such that $b > 0$. No such cutoff is implemented for the largest masses. In Figure 1 we plot the ensemble-averaged $\langle b_{min} \rangle$ and $\langle b_{max} \rangle$. For each figure we average over a set of 10^5 chains sampled from a normal distribution, with each chain containing 2000 particles. We note that the restriction of $b > 0$ causes the ensemble-averaged minimum mass values to be bounded as we increase the width of the distribution (disorder) ξ . Values of the largest ensemble-averaged masses increase linearly with ξ , as expected.

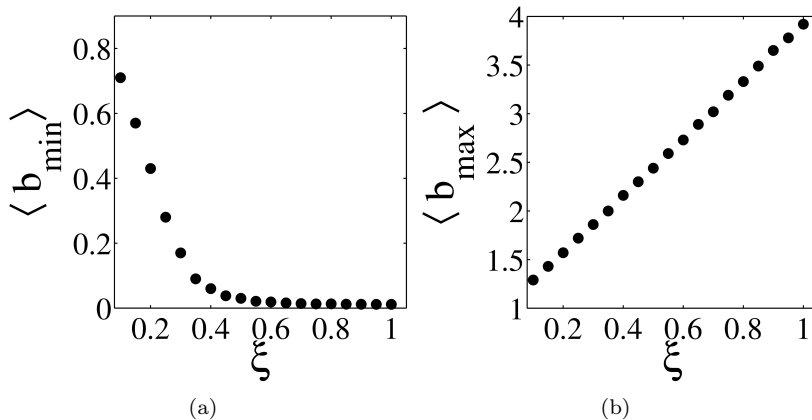


Figure 1: Ensemble-averaged minimum and maximum masses. The masses are sampled from a normal distribution with mean $\bar{b} = 1$ and standard deviation ξ . Each chain contains 2000 particles and the ensemble has 10^5 chains.

For comparison between the three distributions, we match the first two moments of the theoretical probability density functions. By employing three different mass distributions that have the same moments, we may compare the filtering behavior of these systems and investigate the role of the mass distribution. In general, the n^{th} moment of a given distribution $f^{(q)}(b)$ is defined as,

$$M_n^{(q)} = \int_{-\infty}^{\infty} b^n f^{(q)}(b) db, \quad (26)$$

where q is used to identify the specific distribution type. Since only positive masses are permitted, the lower limit of integration may be changed to zero. With $M_1^{(n)} = 1$ and $M_2^{(n)} = 1 + \xi^2$, we calculate the corresponding limits of the uniform distribution to be $1 \pm \sqrt{3}\xi$. For the binary distribution the masses are placed at $1 \pm \xi$. For the binary distribution to be symmetric about the mean, large and small masses are selected with equal probability; the probability of there being j or greater successive equal masses is $\approx 2^{-j}$. Long monodisperse sections which might significantly affect the transmission properties of the chain are thus unlikely.

When comparing the various mass distributions we restrict $\xi \leq 0.5$, neglecting $\approx 2.3\%$ of the normal distribution where $b < 0$. In the context of our parameter study employing only normally distributed masses, we consider $\xi \leq 1$.

3.2 Linear chain filtering

Given an array of $(N + 2)$ random masses (where the end particles have prescribed motion), we numerically solve the eigenvalue problem as described in section 2.2, yielding the $(N \times N)$ eigenvector matrix \mathbf{S} and the N eigenfrequencies $\{\omega_{(j)}\}$ ($j = 1, \dots, N$). With equation (24) we calculate the displacement history $u^{(p)}(\tau_n)$ of particle p at discrete time steps $\tau_n = n\tau$ on the interval $\tau = [0, \tau_{max}]$. The time window is sufficiently large and the scaled time step $d\tau$ is chosen to be small enough to permit sampling at the frequencies of interest. We then perform a discrete Fourier transform to obtain the spectrum of this signal. In particular, we examine the absolute value of the Fourier components, $U^{(p)}(\omega)$. This calculation is performed for particles $p = 1, \dots, M$. The length of the chain $(N + 2)$, the sampling region length M , and the time window τ_{max} are chosen such that the disturbance signal has not reached the end-particle $p = N + 1$ and thus is not reflected back, preventing interference from reflected waves. Additionally, the parameters are chosen such that the high frequencies (with corresponding lower phase velocity) have been given sufficient time to propagate through the sampling region; if the time duration were too short, then the “filtering” could, in fact, only be a measurement artifact.

The spectra of oscillations for the sampled particles may be compactly visualized by the use of a three-dimensional plot projected into a two-dimensional plane. Here we plot in the (p, ω) plane and represent the values of the absolute Fourier components $|U^{(p)}(\omega)|$ in greyscale. At each location p , the $|U^{(p)}(\omega)|$ array of values is normalized to unity (which allows to compare their relative contribution). In our convention, darker shades correspond to larger values with the scaling set such that black corresponds to a Fourier component ≥ 0.2 . This is applied for all of the following figures. For two particular chain arrangements, we obtain Figure 2. We will later show averages over 200 different realizations.

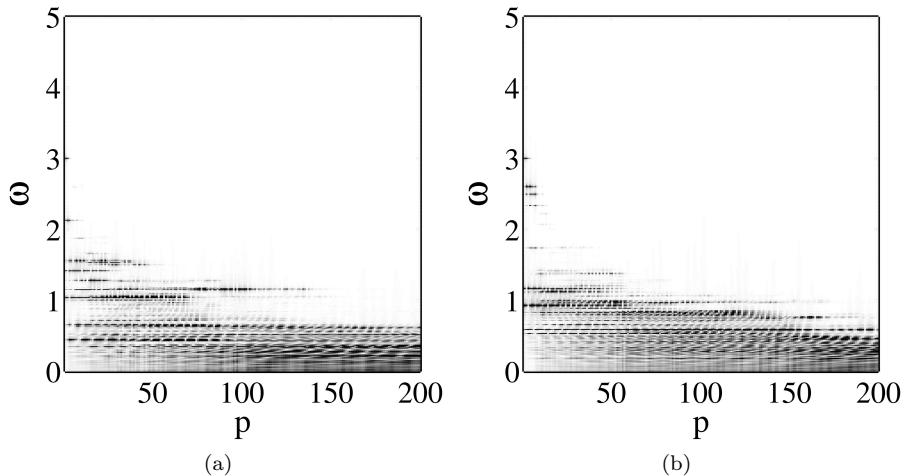


Figure 2: Frequency propagation spectrum as a function of distance (in mean particle diameters) from the source for two instances of a single realization of a normally distributed disordered chain with uniform linear coupling. $\xi = 0.5$, $\omega_o = 3$, $d\tau = 0.0667$, $\tau_{max} = 546.41$, $N = 500$, $M = 200$.

In both of Figures 2a and 2b we note a rapid decrease of the input frequency within several particle diameters from the driver. Following this, we observe the persistence of several lower frequencies ($\omega < \omega_o$) which are dependent on the particular chain arrangement. However, by $p = 200$ we note that the frequency content of the two arrangements is more comparable and frequencies $\omega \gtrsim 0.5$ have absolute Fourier components that are relatively small with respect to $\omega \lesssim 0.5$. This range of propagated frequencies is dependent on the disorder parameter, as investigated in Section 3.2.1.

Examining the evolution of a particular frequency component ω^* as it propagates down the chain, we note the dark and light oscillations (“stitching”) apparent for certain frequencies in both plots of Figure 2. For lower frequencies, the wavelengths of these features match closely with those obtained from the dispersion relation (25) for the perfect chain, as shown in Figure 3. Here, for a single chain realization, we compare the features of the dispersion relation to the spatial filtering behavior. To construct this figure we perform a discrete double Fourier transform of the $u^{(p)}(\tau)$ signal. With this plot we may examine the wavelength λ of the stitching as ω^* is varied. Note the close agreement between the analytical result (black circles) and the data in the low-frequency/long-wavelength limit ($\omega < 0.5$). As the frequency increases, there is significant deviation of the disordered system from the monodisperse chain. The dark horizontal lines change with the particular chain arrangement and correspond to strong, but spatially short excitations, indicating localization of the oscillations at frequency ω^* .

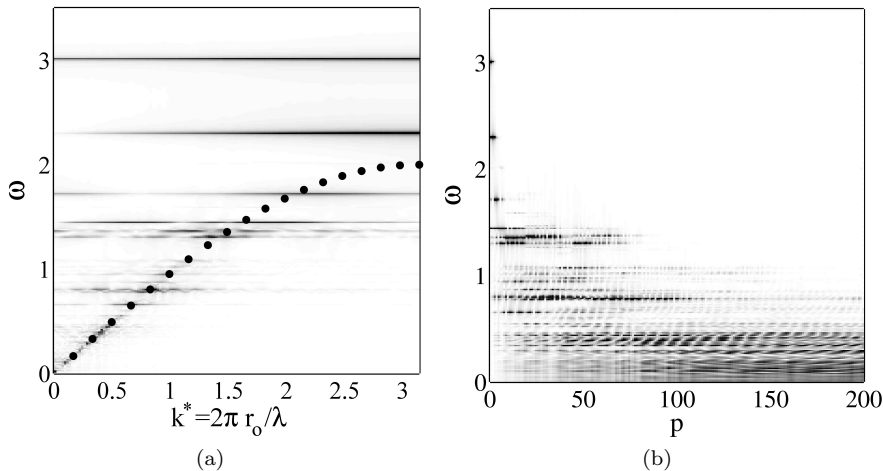


Figure 3: The dispersion relation (a) obtained from the simulation displayed in (b). The black circles are obtained from the perfect chain ($\xi = 0$) dispersion relation (25) at 20 equidistant k^* values. Darker shades correspond to greater magnitude Fourier components.

The light areas of the stitching thus correspond to nodes of the wave, where the magnitude of oscillations at a particular frequency ω^* are insignificant. Based upon the chain arrangement this behavior is more visually apparent at certain frequencies, but Figure 3 confirms that there is a “selected” wavelength associated with the oscillations for intermediate to low frequencies. We note that the stitching is a consequence of the wave component interactions since it is not present in our simulations with perfect chains; in such cases a monochromatic horizontal line is observed to propagate without change (if in the passband $\omega \leq 2$). Simulations of perfect chains produce dispersion plots that exactly match the black circles plotted in Figure 3.

3.2.1 Frequency-filtering of the monodisperse linear chain: normally distributed masses

Here we employ a normal distribution of masses and perform a parameter study on the effects of disorder magnitude ξ and source frequency ω_o . For each set of data, we generate an ensemble of 200 random chains (with different random masses; however, for the equal-mass chain, this has no effect due to lack of random disorder, i.e. $\xi = 0$). Each chain contains $N = 500$ particles and we examine the displacement signal for particles 1 through $M = 200$. Selection of the chain length N and the value of M is based on examining the results of longer systems; for relatively high disorder ($\xi = 0.5$) we note minimal change in the spectrum of transmitted frequencies beyond approximately 200 particles from the excitation source.

By requiring that the signal does not reach the fixed end-particle $p = (N+1)$, a sampling time interval $\tau = [0, \tau_{max}]$ is approximately determined from the analysis of several chain arrangements (“microstates”). If the fixed end is indeed reached in a particular microstate, the reflected signal certainly does not have sufficient time to propagate backwards to the sampling region, $p < M$.

With τ_{max} set, we divide the time span into q steps such that $d\tau = \tau_{max}/q$ is small enough to detect the relevant large frequencies in a given signal. As stated in Section 2.2, a monodisperse linear chain will propagate normalized frequencies $\omega \leq 2$ and we drive the disordered chains at frequencies of this order. We select $q = 8192$ time steps which yields $d\tau \approx 0.0667$ for the given time interval. We note that this time step permits detection of frequencies $\omega \lesssim 47.1$, which is many times greater than the largest eigenfrequencies.

For each realization in the ensemble of disordered chains, we calculate the motion and the Fourier transform for the particles in the sampled region $p < M$. To obtain the ensemble frequency content, we subsequently average over the Fourier transform data for each microstate.

We emphasize that for Sections 3.2.1 through 3.2.2 we are concerned with systems where only the masses are disordered. The coupling stiffnesses $\kappa_{(ij)} = 1$ are the same for all contacts in the chain. In section 3.2.3 we vary the contact stiffnesses along with the particle masses.

Fix ω_o , vary ξ : Here we set the driving frequency $\omega_o = 3.0$ to a constant value and vary the disorder parameter ξ as shown in Figure 4. In this manner we may examine the effect of disorder on the transmitted frequencies. We note that the greyscale values for each subplot are the same, with the absolute Fourier component of magnitude 0.0 corresponding to white and 0.2 or greater appearing black.

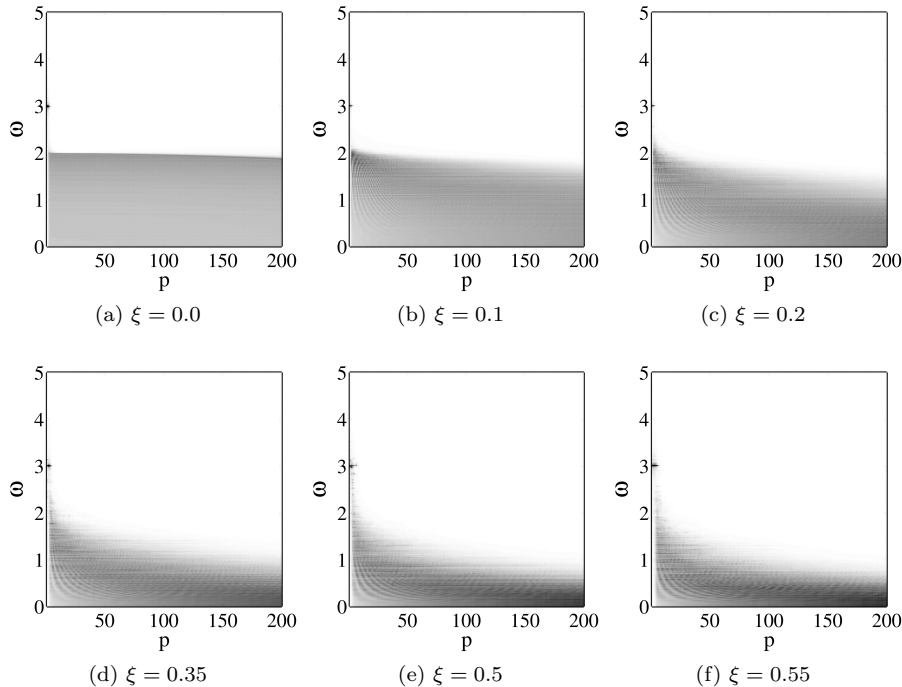


Figure 4: Variation of the disorder parameter ξ . The source frequency $\omega_o = 3.0$ and the other parameters are the same as in Figure 2.

From Figure 4 we note that as the disorder parameter increases (from sub-figures 4a to 4f) there is an associated decrease in the transmission of the relatively higher frequency components. For ξ in the range $[0.1, 0.65]$, we examine the ensemble-averaged spectrum of particle $p = 200$, $\langle |U^{(200)}(\omega)| \rangle$. In accordance with the filtering behavior, the more disordered chains have a greater proportion of their content in the low-frequencies. The inset of Figure 5 depicts $\langle |U^{(200)}(\omega)| \rangle$ for $\xi = 0.3$. Less disordered chains have a flatter profile with the decay occurring closer to $\omega = 2.0$ while more disordered chains display a higher peak and sharper decay. To quantify the effect of disorder on the spectrum width, we measure the frequency $\omega_{1/2}$ at which the curve reaches half its nominal/peak value, depicted in the inset by the dotted lines. This is performed for 10 ensembles at each ξ and plotted in Figure 5.

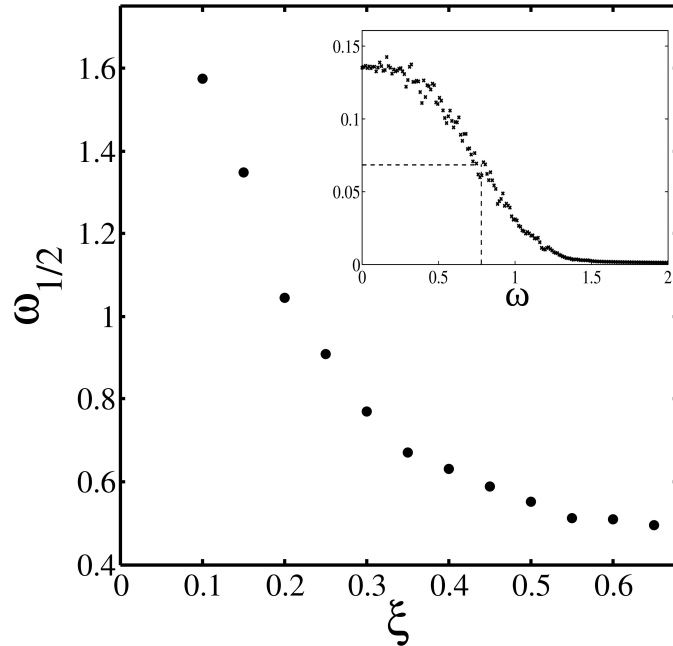


Figure 5: Spectrum-width measure $\omega_{1/2}$ for ξ , obtained from the ensemble-averaged profiles $\langle |U^{(200)}(\omega)| \rangle$. Inset shows the profile of $\langle |U^{(200)}(\omega)| \rangle$ for $\xi = 0.3$

As suggested by the images in Figure 4, increasing ξ leads to an initially rapid change in the bandwidth of transmitted frequencies; as the disorder is increased further, the $(\xi, \omega_{1/2})$ curve flattens and the spectrums appear quite similar. Despite the proportionally greater number of small particles accompanying greater disorder, their presence does not appear to significantly affect the ensemble-averaged signal transmission properties. This is discussed further in Section 3.3.

Fix ξ , vary ω_o : Here we set the disorder parameter at a constant $\xi = 0.3$ and vary the source frequency ω_o . For each driving frequency we employ the same ensemble of 200 normally-distributed random mass chains. Results for six input frequencies are shown in Figure 6.

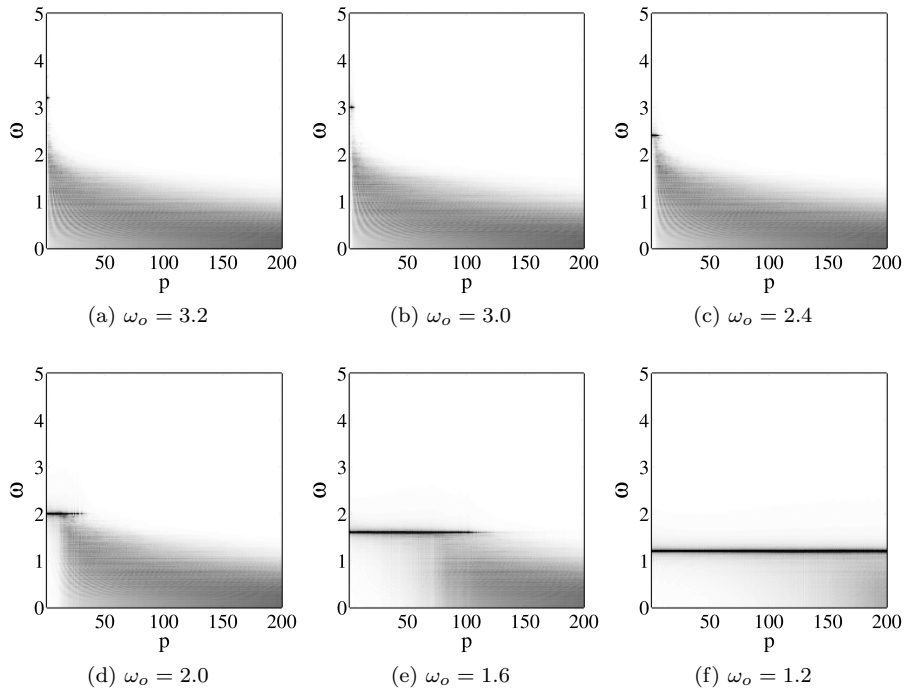


Figure 6: Variation of the source frequency ω_o , for disorder parameter $\xi = 0.3$ and other parameters as in Figure 2.

As suggested by the plots of Figure 4, lower frequency signal components are not as affected by the presence of mass-disorder. This is clearly shown in Figure 6 where the frequency components corresponding to the excitation are shown to propagate further into the system for decreasing ω_o . As evidenced by Figure 3, low frequency (long wavelength) oscillations of disordered arrangements capture the dispersion behavior of ordered systems and thus low frequency inputs propagate similar to the perfect chains. This is discussed further in Section 3.3. Qualitatively similar results are obtained for other values of the disorder parameter ξ .

3.2.2 Frequency-filtering of the linear chain: comparison of mass distributions

Here we compare the results for different mass distributions. As detailed in Section 3.1 we employ normal, uniform, and binary distributions such that the first two moments are matched for a given disorder parameter ξ . In each row of Figure 7 we plot the results for a given distribution.

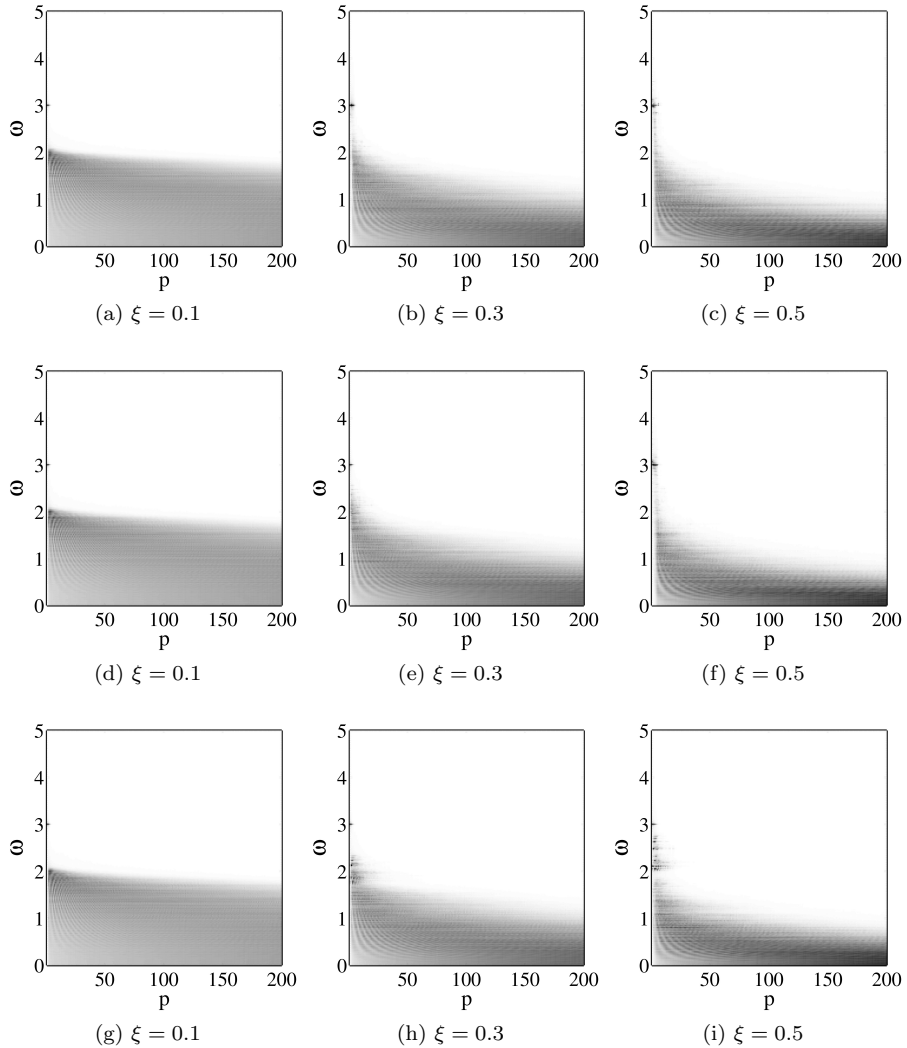


Figure 7: Comparison of normal [(a), (b), (c)], uniform [(d), (e), (f)], and binary mass distributions [(g), (h), (i)] for $\xi = 0.1, 0.3, 0.5$, driven at $\omega_o = 3.0$

Aside from small differences close to the source we observe that the spectrum of transmitted frequencies is approximately the same for the three mass distributions studied at $\xi \leq 0.5$. The binary distribution shows more isolated frequencies penetrating the near-field, giving the figure a “rougher” appearance, but plotting the frequency spectrum $\langle |U^{(p)}(\omega)| \rangle$ for $p > 150$ (data not shown)

reveals no discernible difference between the distributions. The quantitative similarity of the transmission profiles for the binary mass system (as compared to the normal and uniformly distributed systems) suggests that the intermediate mass particles do not have a significant effect; the bulk filtering behavior is related to the interaction between the largest and smallest masses, quantified by the moments of the mass distribution. It is worth noting that higher disorder $\xi > 0.65$ does indeed result in a difference in the profiles $\langle |U^{(p)}(\omega)| \rangle$ for the binary and normal distributions. However, this is expected, as greater ξ values lead to a significant cutoff of the Gaussian tail where $b > 0$; the theoretical moments no longer correspond to the sampled distribution and comparison is no longer appropriate.

3.2.3 Frequency-filtering of the mass- and contact-disordered linear chain

Here we present results for the linearized approximation to the general nonlinear governing equations as valid for small amplitude oscillations. This is equivalent to a linear chain where the mass and contact stiffness are both disordered. The non-dimensional contact stiffness is related to the sizes of the contacting particles as given in (15). Comparison of Figures 8a–8c with the corresponding plots

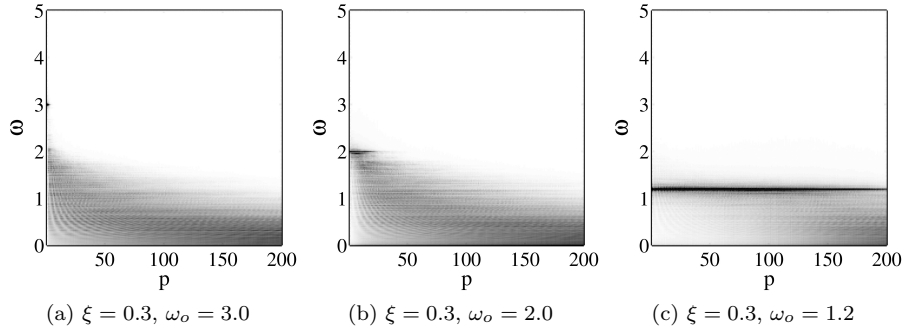


Figure 8: Mass- and contact-disordered chain for $\xi = 0.3$ and $\omega = 3.0, 2.0, 1.2$

of Figure 6 reveals that the addition of contact disorder leads to a more rapid spatial decay of the input frequency ω_o . We also note that the bandwidth of transmitted frequencies is marginally reduced for the contact-disordered chains, as evidenced by plotting the profiles at various downstream locations (plots not shown). However, the shape of the profiles are qualitatively comparable to those of Figure 6.

3.3 Disorder and localization

In this section we discuss how disorder in the one-dimensional chain leads to spatial localization of the eigenmodes. Through the use of a simple fixed-end, non-driven chain, we show that this localization is responsible for the observed filtering behavior of the chains presented above. Although we mainly consider driven chains in this study, the fixed-end chain provides a convenient model system for our heuristic argument concerning high-frequency filtering.

3.3.1 Density of states

In Figure 9 we plot the density of states for various values of the disorder parameter. The eigenvalues for 2000 states of a 500 particle chain are numerically calculated and the density of states is normalized such that the sum of values (for each ξ) is unity, i.e. it represents the probability density function of modes as function of ω . The numerical results are plotted with the analytical result for a perfect chain as given by Sheng [36],

$$\rho(\omega) \sim \frac{1}{\sqrt{4 - \omega^2}}. \quad (27)$$

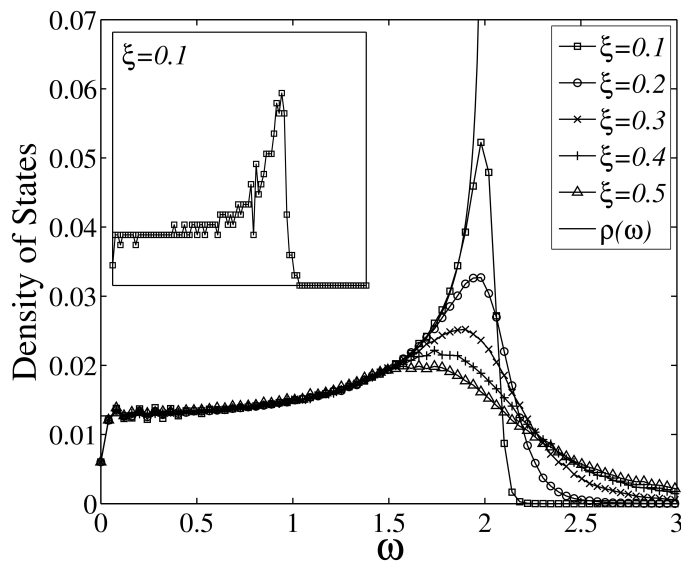


Figure 9: Density of states for mass-disordered chains. The curve $\rho(\omega)$ is the analytical result (27) for the density of states in a monodisperse chain. Inset displays the density of states for a single chain with $\xi = 0.1$.

In Figure 9 the density of states increases as we approach the cutoff frequency $\omega = 2.0$ of the ordered chain. As the disorder is increased, the smaller masses permit higher frequency oscillations and the density of states for frequencies $\omega > 2.0$ accordingly increases. One may observe in Figures 2 and 4 that there is (limited) transmission of frequencies $\omega > 2.0$ for higher disorder; when $\xi = 0$, we see a very sharp cutoff at $\omega = 2.0$.

3.3.2 Localization

From Section 2.2 we recall the eigenvalue problem (17) for the general linear chain. In the case of monodisperse particles, the eigenvectors are sinusoids subject to the condition that the ends remain fixed. This imposes the requirement that the eigenmode wavenumbers are scalar multiples of π/L , where L is the chain length between the pinned ends. For the disordered chain, we observe that eigenmodes of increasing frequency exhibit spatial mode localization. This so-called ‘‘Anderson’’ localization has been observed in many physical contexts including mechanical systems of vibrating masses [19, 32].

Numerically solving the eigenvalue problem for three particular arrangements of a 500 particle random chain ($\xi = 0.5$, uniform stiffness) we plot sample eigenvectors for modes $j = 2, 30, 100, 200, 300, 500$ in Figure 10. The low frequency modes (e.g. Figures 10a and 10b) are similarly shaped for the different chains and are ‘‘extended’’ in nature – the displacements are not localized about a portion of the chain as seen in the higher frequency modes (10c to 10f). In addition to the increased localization of higher frequency modes, we note that the displacements are located at different positions in the chain, indicating sensitivity to the particular mass arrangement. The highest frequency modes approach Dirac–delta functions where only a single particle has a significant displacement (Figure 10f). Physically, the highest frequency modes correspond to smaller mass particles oscillating between two relatively large neighbors. We note that the large peak in the k^{th} highest frequency eigenmode corresponds to the location of the k^{th} smallest mass.

To investigate the effect of mode localization on the filtering behavior of random chains, we simplify the modeling by removing the driving excitation of the end particle. With this fixed–end chain, we consider the time evolution of an initially specified waveform \mathbf{u}_o . The general solution derived in Section 2.2 reduces to

$$\mathbf{u}(x, \tau) = \mathbf{S}\mathbf{C}\mathbf{S}^{-1}\mathbf{u}_o, \quad (28)$$

where \mathbf{C} is a diagonal matrix with $\cos \omega_{(j)}\tau$ as the (j, j) entry. Recall \mathbf{S} to be the matrix of eigenvectors and $\omega_{(j)}$ as the frequency of the j^{th} eigenmode.

3.3.3 Wavenumber spectra evolution with time

Just as high frequencies are observed to be filtered with distance from the driving source, high wavenumber/short wavelength content is observed to decay with time and only long wavelengths persist. Given the displacement history (28) we perform a spatial discrete Fourier transform (DFT) to obtain the wavenumber content by application of the DFT matrix ${}^1\mathbf{F}$:

$$\mathbf{\Upsilon}(k, \tau) \equiv \mathbf{F}\mathbf{u}(x, \tau) = \mathbf{F}\mathbf{S}\mathbf{C}\mathbf{S}^{-1}\mathbf{u}_o. \quad (29)$$

One may also differentiate Eq. (29) with respect to time (the only time dependence hidden in $\mathbf{C} = \mathbf{C}(\tau)$) to phrase this in the form of a master equation

$$\frac{d\mathbf{\Upsilon}}{d\tau} = \mathbf{Q}\mathbf{\Upsilon}, \quad (30)$$

¹Using e.g. the matlab function `dftmtx`.

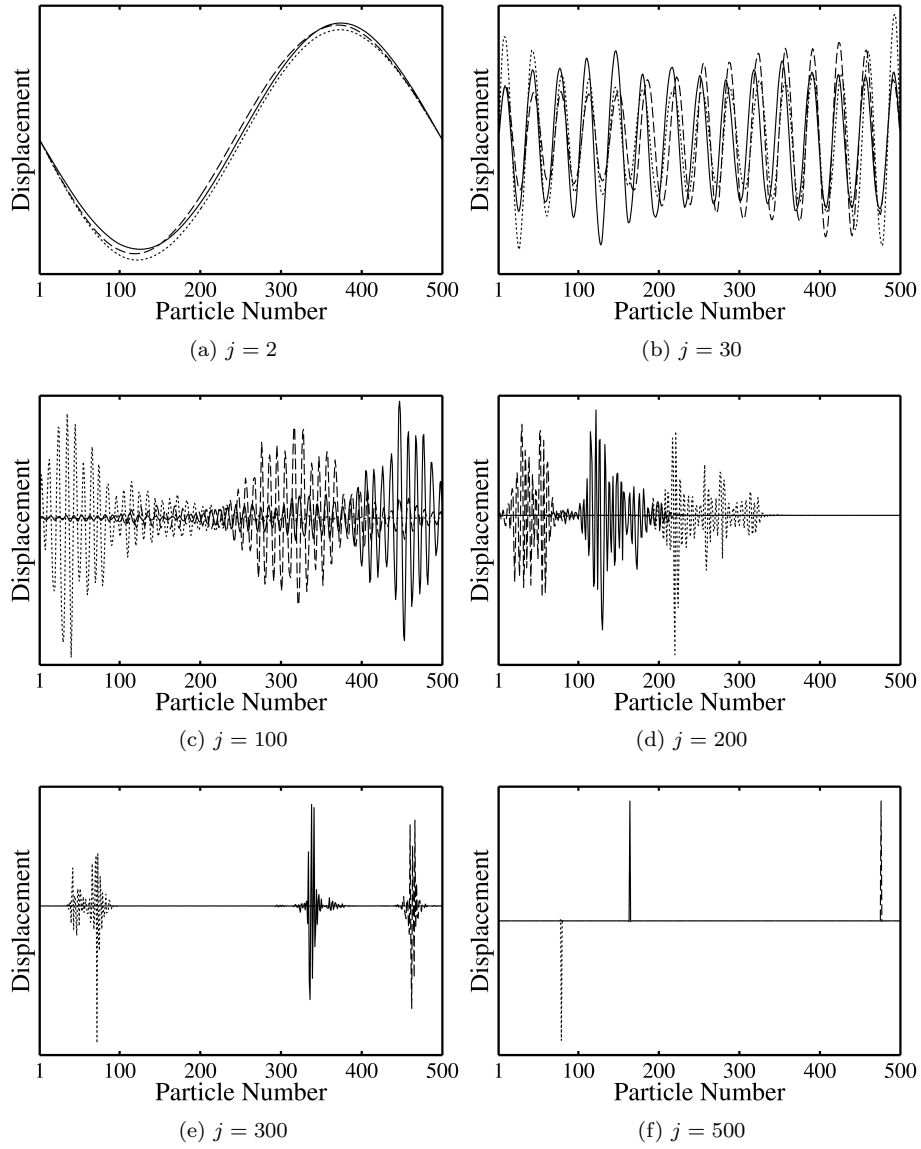


Figure 10: Eigenmode shapes for modes $j = 2, 30, 100, 200, 300, 500$. Each subfigure displays the mode shape for three different random chain arrangements with disorder parameter $\xi = 0.5$.

where $\mathbf{Q}(\tau) \equiv \mathbf{F}\mathbf{S}\mathbf{H}\mathbf{S}^{-1}\mathbf{F}^{-1}$, and $\mathbf{H} = \mathbf{H}(\tau) = (d\mathbf{C}/d\tau)\mathbf{C}^{-1}$ is a diagonal matrix with (j, j) entry $-\omega_{(j)} \tan \omega_{(j)}\tau$. The transition between wavenumber states is determined by the transition matrix \mathbf{Q} .

To examine the evolution of a particular wave component, we imagine prescribing the initial displacement to be a perfect sinusoid, subject to the fixed boundary conditions. Restricting attention to (29), we decompose this initial waveform into the sum of an eigenvector \mathbf{s}_j and a difference vector $\boldsymbol{\chi}$. Thus, we write

$$\boldsymbol{\Upsilon}(k, \tau) = \mathbf{F}\mathbf{S}\mathbf{C}\mathbf{S}^{-1}(\mathbf{s}_j + \boldsymbol{\chi}), \quad (31)$$

which simplifies to

$$\boldsymbol{\Upsilon}(k, \tau) = \cos(\omega_j\tau)\mathbf{F}\mathbf{s}_j + \mathbf{F}\mathbf{S}\mathbf{C}\mathbf{S}^{-1}\boldsymbol{\chi}. \quad (32)$$

If the initially inserted waveform has a long wavelength as compared to the constituent particle sizes, see Fig. 10(a,b), the decomposition suggests that $\mathbf{s}_j \approx \mathbf{u}_0$ and $\boldsymbol{\chi}$ is relatively insignificant, leaving $\boldsymbol{\Upsilon} \approx \cos(\omega_j\tau)\mathbf{F}\mathbf{s}_j$. The product $\mathbf{F}\mathbf{s}_j$, yielding the distribution of $\boldsymbol{\Upsilon}$ in k -space, would only feature contributions from a small number of long wavelengths and the wavenumber content remains qualitatively similar – oscillating in time with frequency ω_j .

Conversely, if we consider inserting a small wavelength/high frequency sinusoid \mathbf{u}_0 , the first term of (32) is the Fourier transform of an (arbitrary) high-frequency eigenmode (e.g. Figure 10f), which contains contributions from all wavenumbers (due to its peaked, localised nature). Thus, we observe the tendency of a high-frequency mode wave to spread (distribute) its wavenumber content across all wavenumbers. Since a strongly localized \mathbf{s}_j features very few non-zero entries, one has $\boldsymbol{\chi} = \mathbf{u}_0 - \mathbf{s}_j \approx \mathbf{u}_0$, and the second term of (32) is approximately equal to $\mathbf{F}\mathbf{S}\mathbf{C}\mathbf{S}^{-1}\mathbf{u}_0$, while the first is rather insignificant (alternatively one could have started directly with setting the first term to zero).

The product $\mathbf{S}^{-1}\mathbf{u}_0$ yields a vector $\mathbf{q}(\mathbf{u}_0)$ describing the linear combination of eigenvectors comprising the original waveform (for a particular chain arrangement). Writing out the terms of this matrix product, we see

$$\mathbf{F}\mathbf{S}\mathbf{C}\mathbf{S}^{-1}\mathbf{u}_0 = [q_1 \cos(\omega_1\tau)]\mathbf{F}\mathbf{s}_1 + \dots + [q_N \cos(\omega_N\tau)]\mathbf{F}\mathbf{s}_N. \quad (33)$$

Thus, the coefficients q_1, \dots, q_N determine the amplitude of oscillations for each term and $\mathbf{F}\mathbf{s}_j$ describes how the term's wavenumber content is distributed in k -space. To observe the relative magnitude of the coefficients over a range of input \mathbf{u}_0 , we calculate $\mathbf{q}(\mathbf{u}_0)$ for 200 chains of $N = 500$ particles with $\xi = 0.5$. In Figure 11 we plot the results in greyscale, where darker shades represent larger absolute values of the components. Increasing k along the horizontal axis corresponds with shorter wavelength initial waveforms. Vertical cross-sections (fixed k) yield the components \mathbf{q} for the inserted waveform. The sharp, dark diagonal in the bottom left of the figure confirms that the coefficients corresponding to lower frequencies/longer wavelengths have greater absolute value and that long wavelengths persist. As the input wavelength is decreased, however, the relative magnitude of the coefficients is decreased and the distribution becomes spread, consistent with simulation observations in both the fixed-end and driven chains. Thus, from this simple decomposition, it is clear that mode localization is responsible for the filtering of high-frequency content in the presence of mass-disorder.

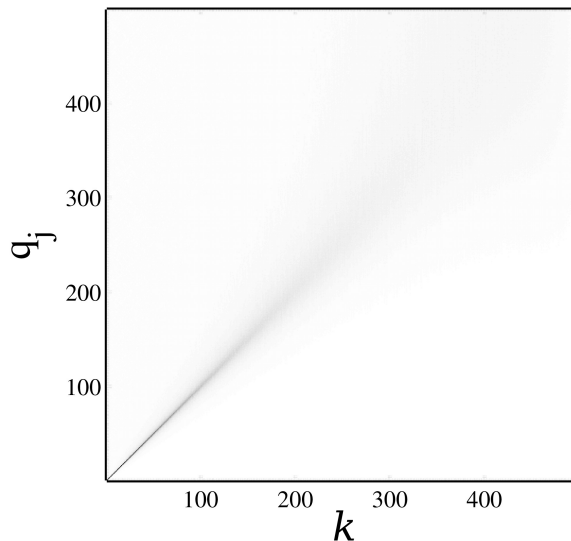


Figure 11: Absolute values of the components of \mathbf{q} (see text) for varied input waveforms \mathbf{u}_o , which for increasing k along the horizontal axis become wider spread out (lower shades of grey) across the eigenmodes. Results are produced for an ensemble of 200 chains of $N = 500$ particles with $\xi = 0.5$

3.4 Frequency-filtering of the nonlinear chain

Similar to the linear chain, in Section 3.4.1 we perform a parameter study of ξ and ω_o for a system of normally-distributed masses with Hertzian interaction. Due to the nonlinearity in the contact law, we also consider the driving amplitude ϵ . We note that the nonlinear chain is, in general, disordered in both mass and contact properties. In Section 3.4.2 we investigate nonlinear chains with uniform contact coupling, isolating the effect of mass-disorder.

3.4.1 Frequency-filtering of the nonlinear chain: normally distributed masses

Fix ω_o , vary ξ : Here we set the driving frequency $\omega_o = 3.0$ and present the spectra for three values of the disorder parameter ξ in Figure 12.

We may compare this nonlinear chain with the results of 3.2.3, where a linear contact model is employed for the mass- and contact-disordered chain. As observed in the linear system, increased disorder leads to stronger filtering of the high-frequency components. However, the profiles of transmitted frequencies are qualitatively different for the nonlinear chain. In Figure 13 we plot the transmission profiles $\langle |U^{(200)}(\omega)| \rangle$ for a general nonlinear (with contact-disorder), a contact-ordered nonlinear (see Section 3.4.2), and a contact-disordered linear chain (Section 3.2.3).

We observe that the profiles for the nonlinear chains display a sharp peak at the low frequencies, while the linear chain exhibits a flatter profile. The magnitudes of the intermediate frequency components are accordingly less in the nonlinear chain. However, we note that by changing ϵ the oscillation amplitudes

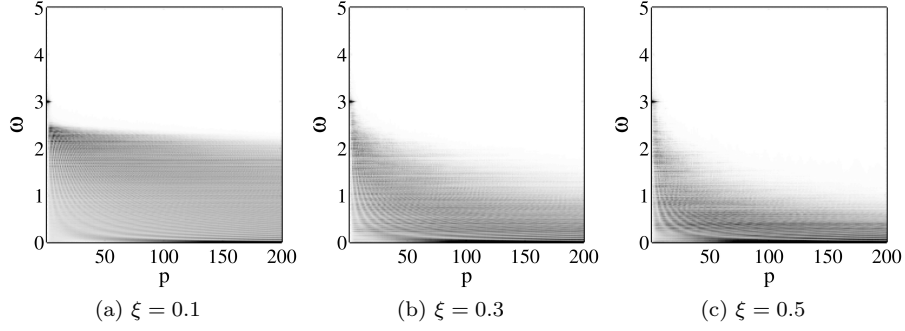


Figure 12: Variation of disorder parameter ξ for a normal distribution of masses and Hertzian contact. Source frequency is $\omega_o = 3.0$ and the relative driving amplitude is moderate, $\epsilon = 0.05$; for a comparison of different ϵ , see Fig. 16.

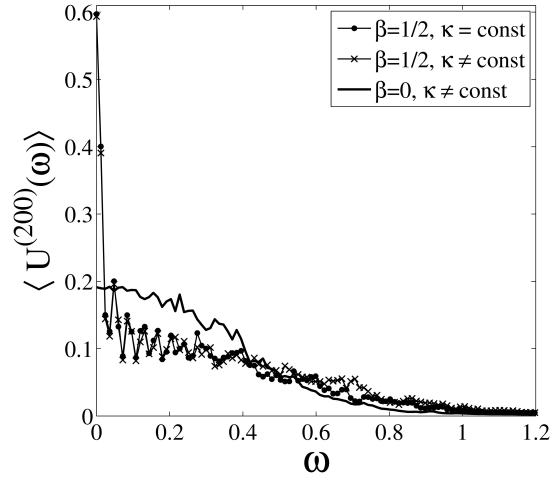


Figure 13: Frequency spectrum at particle $p = 200$ for contact-disordered nonlinear, contact-ordered nonlinear, and contact-disordered linear chain. Parameters are $\xi = 0.5$, $\omega_o = 3.0$ and $\epsilon = 0.05$ for the nonlinear chains.

will decrease such that we approach behavior that is captured by the linearized model. This is examined later, see Fig. 16.

An apparent feature of the nonlinear spectra is the “zig-zag” for $\omega < 0.2$. This is not an artifact of the sampling rate or time period and the feature persists upon ensemble-averaging. At a particular ξ and ω_o the only simulation parameter that affects the height of the peaks is the driving amplitude ϵ (see Figure 16), which characterizes the strength of the nonlinearity through the displacements from equilibrium. In Figure 14 we alter ξ and ω_o to show that changing the disorder (at fixed ω_o) does not have any effect on the ω location of the zig-zags. Similarly, changing ω_o does not appear to have a significant effect on the locations for $\omega < 0.2$. The reason for the particular locations remains an open question.

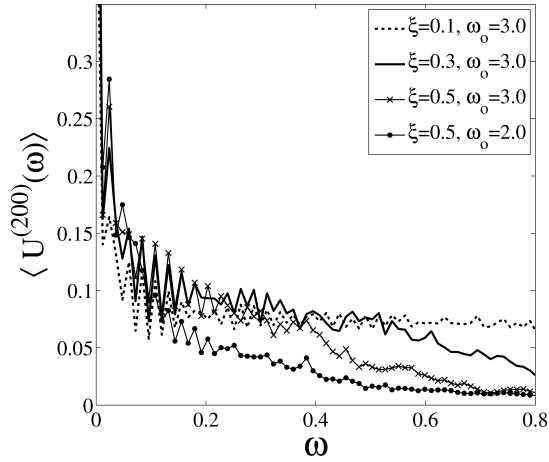


Figure 14: Ensemble-averaged frequency spectrum at particle $p = 200$ for the nonlinear chain with $\epsilon = 0.05$. Note that changes in ξ and ω_o do not have a significant effect on the location of the “zig-zag” features for low frequencies.

Fix ξ , vary ω_o Here we set the disorder parameter to $\xi = 0.5$ and change the driving frequency ω_o . Results are plotted in Figure 15.

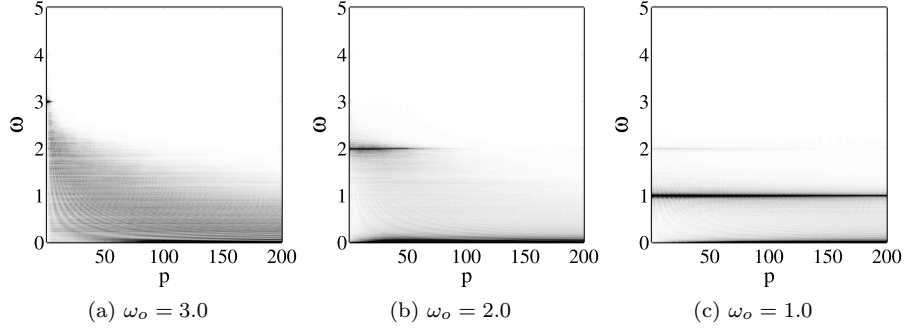


Figure 15: Variation of source frequency ω_o . Disorder parameter is $\xi = 0.3$ and $\epsilon = 0.05$.

As in the linear chain we see that lower frequency signals are not as sensitive to the disorder of the chain and the input frequency propagates further into the system. In Figure 15c we note the appearance of a harmonic at $\omega = 2\omega_o$. This frequency doubling harmonic (among others not visible due to the greyscale selection) is a general feature of nonlinear oscillations and is observed in all the simulations. Again we see that the nonlinear chain with an appropriately large excitation ($\epsilon = 0.05$ in this figure) experiences a sharp profile for $\omega \ll 1$. The penetration distance of the input frequency (e.g. for $\omega_o = 2.0$) is not affected by the driving amplitude ϵ as varying this parameter over several orders of magnitude resulted in negligible difference in the decay of this component.

Different driving amplitudes Here, the value of the non-dimensional driving amplitude ϵ is varied over several orders of magnitude: $\epsilon = 0.1, 0.05, 5 \times 10^{-3}, 5 \times 10^{-4}$. As noted with respect to equation (9), the non-dimensional value of ϵ measures the strength of the agitation provided by the driving with respect to the compressive external force on the chain. Thus, small values of ϵ correspond to systems with small driving and/or large confining stress. The largest driving amplitudes are set by the requirement that no contacts may open in the chain, giving ϵ_{max} to be on the order of the characteristic overlap length scale. Simulations check this contact condition to avoid the nonlinearities associated with transient interactions.

Since the greyscale plots are qualitatively similar to prior figures (e.g. Fig 12c) and do not resolve the fine details of the transmission profiles, we plot $\langle |U^{(200)}(\omega)| \rangle$ in Figure 16. We note that by decreasing the driving amplitude ϵ , we decrease the magnitude of the lowest frequency components. For $\epsilon \rightarrow 0$, the profiles approach that seen in the linear chain (shown in Figure 13), which is consistent with the linearization performed about the equilibrium positions. The asymptotic approach to linear behavior of a compressed granular system was noted experimentally by Sinkovits *et al.* [37]. It is also apparent that greater ϵ causes the height of the “zig-zag” peaks for $\omega < 0.3$ to grow, enforcing that this is an effect associated with the contact nonlinearity.

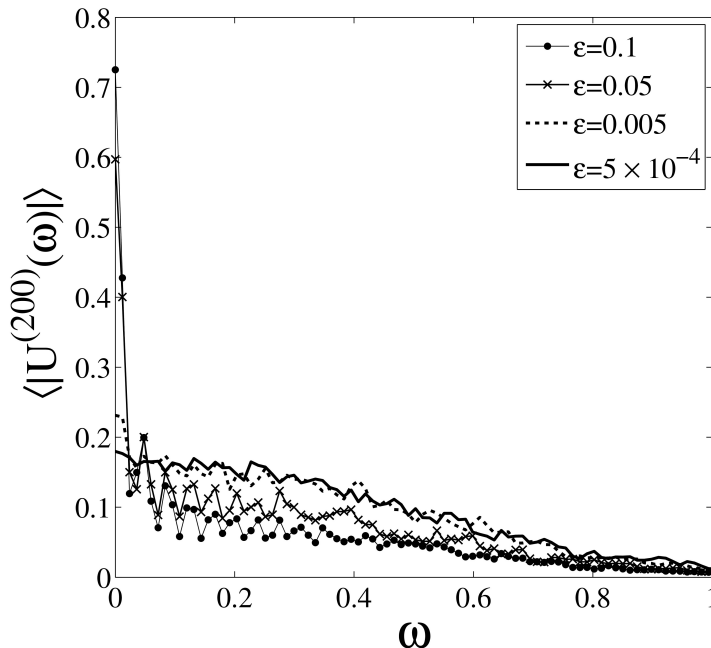


Figure 16: Frequency spectrum at particle $p = 200$ for varied driving amplitude ϵ . Source frequency is $\omega_o = 3.0$ and $\xi = 0.5$.

3.4.2 Removal of contact disorder

In a numerical realization of the monodisperse, mass-disordered setup proposed in Section 2.1.3 we remove the contact disorder in the Hertzian chain by setting

all interaction stiffnesses to $\kappa_{(i,j)} = 1$. The frequency spectra for $p = 200$ were previously plotted in Figure 13. Inspection of the corresponding curves reveals that contact disorder reduces the magnitude of the frequency components in the intermediate frequency range. The profiles are quite comparable for the smallest frequencies, but for $\omega > 0.4$ the spectrum for constant contact stiffness lies slightly above that of the contact-disordered case. As noted prior, similar results were obtained for the linear chains when the effects of contact disorder were considered.

4 Conclusions

In this study we examined the frequency transmission properties of driven, disordered one-dimensional systems. Beginning from a general power law force-displacement relation, we investigated the behavior of pre-compressed chains, where particles interact through linear or nonlinear (Hertzian) contacts. Disordered chains behave like a low-pass frequency filter, permitting the propagation of low frequency signals while the higher frequency components decay with distance from the source. The signal transmission is studied as a function of the input frequency, disorder magnitude, and the choice of contact model (i.e. linear, Hertzian). As more disorder is imposed on the system we observe that the higher relative frequencies are filtered closer to the source/driver and only low-frequencies propagate in the chain. However, the results also suggest that there exists a threshold disorder after which only small changes in the ensemble-averaged properties are noted. By driving systems at various frequencies we observe that lower-frequency signals are less sensitive to the chain arrangements and the input signal propagates further. In the context of the linear chain, we relate the filtering behavior to the localization of eigenmodes in the presence of disorder. One may imagine applications exploiting disorder effects could be pursued in the spirit of [5, 9, 12, 13, 25, 31, 38, 40] where such systems were engineered to produce a desired output.

Chains composed of random, linear, contact-ordered masses sampled from different (normal, uniform, and binary) mass-distributions were compared. The disorder parameter was restricted to $\xi \leq 0.5$ to ensure that only a small portion of the normal distribution ($b < 0$) was neglected. The quantitative agreement between the ensemble-averaged results between the binary and continuous distributions suggests that knowledge of the first two moments of the mass distribution is sufficient for characterizing the bulk filtering properties of these simple systems; the effect of intermediate masses is minimal.

Comparison of the nonlinear and linear systems reveals that both systems filter high frequencies in a similar manner with a decaying envelope of transmitted frequencies. However, the nonlinear chains have frequency spectra that contain much larger relative contributions from the lowest frequency components, indicated by the dramatic difference in the spectra at locations downstream from the driver. By altering the non-dimensional driving amplitude ϵ , we were able to affect the strength of the nonlinearities present; with a sufficiently small value (corresponding to small driving amplitude and/or large external compression), we recover the linear system behavior.

We examined the effect of isolated mass-disorder and the combination of mass- and contact-disorder in both linear and nonlinear chains. Results were qualitatively similar to systems with only mass-disorder; in both cases the inclusion of contact disorder was relatively small, leading to slightly lower relative magnitudes of transmitted frequencies.

In comparing the high-frequency filtering properties of the random one-dimensional systems to the three-dimensional packings of Mouraille and Ludwig [28] we note the importance of the contact geometry in their observations. Beginning from a perfect crystalline geometry, small perturbations in particle size are introduced, which created significant and dominating disorder effects in the system. The disorder (as quantified here by the distribution of particle masses) was indeed very small ($\xi \approx 0.007$) and our simulations on one-

dimensional systems with disorder of this magnitude reveal no difference from perfect, monodisperse systems. This underlies the strong nonlinear effect of minimal compression and potentially transient contacts. In our consideration of compressed chains, we have avoided geometry-induced disorder. However, if the chains were subject to very little pre-compression (approaching Nesterenko's sonic vacuum) [10, 29, 34], the length scale of the particle-size perturbation and the contact overlap length scale would be of the same order and strong nonlinearities could be introduced. We emphasize that we did not pursue such weakly confined systems.

Our observations about disordered one-dimensional systems may furnish clues about the role of disorder in higher-dimensional physical systems, namely the relative importance of geometry and the connection between microscale (e.g. contact length scale) properties and those at the system length scale. The investigation of this micro-macro connection and a host of nonlinear effects associated with weak pre-compression and geometrical disorder remains a rich area warranting further study.

Acknowledgements We thank S. Sterl for careful proofreading and testing of the theory. This research is supported by VICI Project No. 10828/NWO-STW.

A Appendix 1: Orthogonality proof

In direct notation, for eigenvalue/eigenvector j the statement of the dimensionless eigenvalue problem is,

$$\mathbf{A}\mathbf{s}_{(j)} = \omega_j^2 \mathbf{s}_{(j)}. \quad (34)$$

With $\mathbf{A} = -\mathbf{M}^{-1}\mathbf{K}$ we have

$$\mathbf{M}^{-1}\mathbf{K}\mathbf{s}_{(j)} = -\omega_j^2 \mathbf{s}_{(j)} \quad (35)$$

or,

$$\mathbf{K}\mathbf{s}_{(j)} = -\omega_j^2 \mathbf{M}\mathbf{s}_{(j)} \quad (36)$$

Similarly for eigenvector k , we have

$$\mathbf{K}\mathbf{s}_{(k)} = -\omega_k^2 \mathbf{M}\mathbf{s}_{(k)} \quad (37)$$

Taking the transpose of (37),

$$\mathbf{s}_{(k)}^T \mathbf{K}^T = -\omega_k^2 \mathbf{s}_{(k)}^T \mathbf{M}^T \quad (38)$$

Since both \mathbf{K} and \mathbf{M} are symmetric drop the transpose and then right multiply by $\mathbf{s}_{(j)}$,

$$\mathbf{s}_{(k)}^T \mathbf{K}\mathbf{s}_{(j)} = -\omega_k^2 \mathbf{s}_{(k)}^T \mathbf{M}\mathbf{s}_{(j)} \quad (39)$$

Similarly, left multiply (36) by $\mathbf{s}_{(k)}^T$

$$\mathbf{s}_{(k)}^T \mathbf{K}\mathbf{s}_{(j)} = -\omega_j^2 \mathbf{s}_{(k)}^T \mathbf{M}\mathbf{s}_{(j)} \quad (40)$$

Subtract (40) from (39),

$$(\omega_j^2 - \omega_k^2) \mathbf{s}_{(k)}^T \mathbf{M}\mathbf{s}_{(j)} = 0 \quad (41)$$

If $\omega_k^2 \neq \omega_j^2$ we are left with the orthogonality statement,

$$\mathbf{s}_{(k)}^T \mathbf{M} \mathbf{s}_{(j)} = 0 \quad (j \neq k) \quad (42)$$

If $j = k$, the quantity $\mathbf{s}_{(j)}^T \mathbf{M} \mathbf{s}_{(j)} = d_{(j)} \neq 0$. Scaling each eigenvector $\mathbf{s}_{(j)}$ by $\sqrt{d_{(j)}}$, we generate an orthonormal set.

B Appendix 2: Hertz contact model

With $\beta = 1/2$ we obtain the Hertz contact model and the interparticle forces are dependent on the size and material properties of the constituent particles in the following way [18]:

$$\tilde{\kappa}_{(i,j)} = \tilde{Y}_{(i,j)} \left[\frac{\tilde{r}_i \tilde{r}_j}{\tilde{r}_i + \tilde{r}_j} \right]^{1/2}, \quad (43)$$

where

$$\tilde{Y}_{(i,j)}^{-1} = \frac{3}{4} \left(\frac{1 - \nu_i^2}{\tilde{E}_i} + \frac{1 - \nu_j^2}{\tilde{E}_j} \right). \quad (44)$$

\tilde{E}_i and ν_i are the elastic modulus and Poisson's ratio, respectively, of the material composing particle i . The formulation was presented for spheres but is noted to be appropriate for non-spheres as well [18]. In what follows we choose the same material for all particles and $\tilde{Y}_{(i,j)} = \tilde{Y}$ is independent of the contact in consideration,

$$\tilde{Y}^{-1} = \frac{3}{2} \left(\frac{1 - \nu^2}{\tilde{E}} \right). \quad (45)$$

We have previously defined the characteristic length $\tilde{\ell} = \tilde{\Delta}_o$ to be the equilibrium contact overlap of two particles of the mean mass \tilde{m}_o . We first find the characteristic stiffness of this contact,

$$\tilde{\kappa}_o = \frac{\tilde{E}}{1 - \nu^2} \left[\frac{2\tilde{m}_o}{243\pi\tilde{\rho}} \right]^{1/6}. \quad (46)$$

With the initial overlaps defined by (3), we have,

$$\tilde{\Delta}_o = \left(\frac{\tilde{P}}{\tilde{\kappa}_o} \right)^{2/3} \quad (47)$$

The characteristic time is,

$$\tilde{t}_c = \frac{1}{\tilde{\Delta}_o^{1/4}} \sqrt{\frac{1 - \nu^2}{\tilde{E}}} \left[\frac{243\pi\tilde{\rho}\tilde{m}_o^5}{2} \right]^{1/12}. \quad (48)$$

The scaled stiffness ratio at contact (i, j) simplifies to,

$$\kappa_{(i,j)} = \frac{\tilde{\kappa}_{(i,j)}}{\tilde{\kappa}_o} = \sqrt{\frac{2}{b^{(i)1/3} + b^{(j)1/3}}} \left(b^{(i)} b^{(j)} \right)^{1/6}. \quad (49)$$

For a general contact, the equilibrium overlap given by (3) is,

$$\tilde{\Delta}_{(i,j)} = \left(\frac{\tilde{P}}{\tilde{\kappa}_{(i,j)}} \right)^{2/3}. \quad (50)$$

Dividing by our length scale $\tilde{\Delta}_o$, the characteristic contact overlap in equilibrium,

$$\Delta_{(i,j)} = \kappa_{(i,j)}^{-2/3}. \quad (51)$$

References

- [1] P.W. Anderson. Absence of diffusion in certain random lattices. *Phys. Rev.*, 109(5):1492–1505, 1958.
- [2] C. Coste and B. Gilles. On the validity of hertz contact law for granular material acoustics. *Eur. Phys. J. B*, 7:155–168, 1999.
- [3] C. Daraio, V.F. Nesterenko, E.B. Herbold, and S. Jin. Energy trapping and shock disintegration in a composite granular medium. *Phys. Rev. Lett.*, 96:058002, 2006.
- [4] P. Dean. On disordered one-dimensional crystals. *Proc. Phys. Soc.*, 73:413–421, 1959.
- [5] R.L. Doney and S. Sen. Impulse absorption by tapered horizontal alignments of elastic spheres. *Phys. Rev. E*, 72:041304, 2005.
- [6] Robert Doney and Surajit Sen. Decorated, Tapered, and Highly Nonlinear Granular Chain. *Physical Review Letters*, 97(15):APS—4, 2006.
- [7] F.J. Dyson. The dynamics of a disordered linear chain. *Phys. Rev.*, 92(6):1331–1338, 1953.
- [8] F. Fraternali, M.A. Porter, and C. Daraio. Optimal design of composite granular protectors. *Mech. Adv. Mater. Struct.*, 17:1–19, 2010.
- [9] M. Gharib, A. Celik, and Y. Hurmuzlu. Shock absorption using linear particle chains with multiple impacts. *J. Appl. Mech.*, 78(3):031005, 2011.
- [10] L.R. Gomez, A. Turner, M. van Hecke, and V. Vitelli. Shocks near jamming. *Phys. Rev. Lett.*, 108:058001, 2012.
- [11] H.E. Hall. *Solid State Physics*. John Wiley & Sons Ltd., London, 1974.
- [12] U. Harbola, A. Rosas, A.H. Romero, M. Esposito, and K. Lindenberg. Pulse propagation in decorated granular chains: an analytical approach. *Phys. Rev. E*, 80:051302, 2009.
- [13] U. Harbola, A. Rosas, A.H. Romero, and K. Lindenberg. Pulse propagation in randomly decorated chains. *Phys. Rev. E*, 82:011306, 2010.
- [14] E.B. Herbold, J. Kim, V.F. Nesterenko, S.Y. Wang, and C. Daraio. Pulse propagation in a linear and nonlinear diatomic periodic chain: effects of acoustic frequency band-gap. *Acta Mech.*, 205:85–103, 2009.

- [15] X. Jia, C. Caroli, and B. Velicky. Ultrasound propagation in externally stressed granular media. *Physical Review Letters*, 82(9):1863–1866, 1999.
- [16] S. Job, F. Melo, A. Sokolow, and S. Sen. Solitary wave trains in granular chains: experiments, theory, and simulations. *Gran. Matt.*, 10:13–20, 2007.
- [17] J.A. Judge, B.H. Houston, D.M. Photiadis, and P.C. Herdic. Effects of disorder in one- and two-dimensional micromechanical resonator arrays for filtering. *Journal of Sound and Vibration*, 290:1119–1140, 2006.
- [18] L. Landau and E. Lifschitz. *Theory of elasticity*. MIR, Moscow, 1967.
- [19] M. Leibig. Model for the propagation of sound in granular materials. *Phys. Rev. E*, 49(2):1647–1656, 1994.
- [20] E.H. Lieb and D.C. Mattis. *Mathematical Physics in One Dimension. Exactly soluble models of interacting particles*. Academic Press, New York, 1966.
- [21] S. Luding, E. Clément, A. Blumen, J. Rajchenbach, and J. Duran. Studies of columns of beads under external vibrations. *Phys. Rev. E*, 49(2):1634, 1994.
- [22] M. Manciu, S. Sen, and A. J. Hurd. The propagation and backscattering of soliton-like pulses in a chain of quartz beads and related problems. (i). Propagation. *Physica A*, 274:588–606, 1999.
- [23] M. Manciu, S. Sen, and A. J. Hurd. The propagation and backscattering of soliton-like pulses in a chain of quartz beads and related problems. (ii). Backscattering. *Physica A*, 274:607–618, 1999.
- [24] M. Manciu, S. Sen, and A.J. Hurd. Impulse propagation in dissipative and disordered chains with power-law repulsive potentials. *Physica D*, 157:226–240, 2001.
- [25] F. Melo, S. Job, F. Santibanez, and F. Tapia. Experimental evidence of shock mitigation in a hertzian tapered chain. *Phys. Rev. E*, 73:041305, 2006.
- [26] E.W. Montroll and R.B. Potts. Effect of defects on lattice vibrations. *Phys. Rev.*, 100(2):525–543, 1955.
- [27] O. Mouraille. *Sound propagation in dry granular materials: discrete element simulations, theory, and experiments*. PhD thesis, Universiteit Twente, 2009.
- [28] O. Mouraille and S. Luding. Sound wave propagation in weakly disperse polydisperse granular materials. *Ultrasonics*, 48(6–7):498–505, 2008.
- [29] V.F. Nesterenko. Propagation of nonlinear compression pulses in granular media. *J. Appl. Mech. Tech. Phys.*, 24:733–743, 1983.
- [30] L. Ponson, N. Boechler, Y.M. Lai, M.A. Porter, P.G. Kevrekidis, and C. Daraio. Nonlinear waves in disordered diatomic granular chains. *Physical Review E*, 82:021301, 2010.

- [31] T. Pöschel and N. V. Brilliantov. Extremal collision sequences of particles on a line: optimal transmission of kinetic energy. 2000.
- [32] H.B. Rosenstock and R.E. McGill. Vibrational modes of disordered linear chains. *J. Math. Phys.*, 3(1):200–202, 1962.
- [33] H. Schmidt. Disordered one–dimensional crystals. *Phys. Rev.*, 105(2):425–441, 1957.
- [34] S. Sen, J. Hong, J Bang, E. Avalos, and R. Doney. Solitary waves in the granular chain. *Physics Reports*, 462:21–66, 2008.
- [35] S. Sen, M. Manciu, and J.D. Wright. Solitonlike pulses in perturbed and driven hertzian chains and their possible applications in detecting buried impurities. *Physical Review E*, 57(2):2386–2397, 1998.
- [36] P. Sheng. *Introduction to Wave Scattering, Localization and Mesoscopic Phenomena*. Springer Verlag, Berlin, 2006.
- [37] R. S. Sinkovits and S. Sen. Nonlinear Dynamics in Granular Columns. *Phys. Rev. Lett.*, 74(14):2686, 1995.
- [38] A. Sokolow, J.M. Pfannes, R.L. Doney, M. Nakagawa, J.H. Agui, and S. Sen. Absorption of short duration pulses by small, scalable, tapered granular chains. *Appl. Phys. Lett.*, 87:254104, 2005.
- [39] V. Tournat, V.E. Gusev, and B. Castagnède. Self–demodulation of elastic waves in a one–dimensional granular chain. *Physical Review E*, 70(2):056603, 2004.
- [40] D.T. Wu. Conservation principles in solitary impulse propagation through granular chains. *Physica A*, 315:194–202, 2002.
- [41] J.M. Ziman. *Principles of the Theory of Solids*. Cambridge University Press, 2nd edition, 1972.